

Design of a new dynamical core for global atmospheric models based on some efficient numerical methods

WANG Bin¹, WAN Hui¹, JI Zhongzhen¹, ZHANG Xin², YU Rucong¹,
YU Yongqiang¹ & LIU Hongtao¹

1. State Key Laboratory of Numerical Modeling for Atmospheric Sciences and Geophysical Fluid Dynamics,
Institute of Atmospheric Physics, Chinese Academy of Sciences, Beijing 100029, China;

2. Department of Computational Mathematics, Academy of Mathematics and System Sciences, Peking
University, Beijing 100871, China

Correspondence should be addressed to Wang Bin (email: wab@lasg.iap.ac.cn)

Received October 15, 2003

Abstract A careful study on the integral properties of the primitive hydrostatic balance equations for baroclinic atmosphere is carried out, and a new scheme to design the global adiabatic model of atmospheric dynamics is presented. This scheme includes a method of weighted equal-area mesh and a fully discrete finite difference method with quadratic and linear conservations for solving the primitive equation system. Using this scheme, we established a new dynamical core with adjustable high resolution acceptable to the available computer capability, which can be very stable without any filtering and smoothing. Especially, some important integral properties are kept unchanged, such as the anti-symmetries of the horizontal advection operators and the vertical convection operator, the mass conservation, the effective energy conservation under the standard stratification approximation, and so on. Some numerical tests on the new dynamical core, respectively regarding its global conservations and its integrated performances in climatic modeling, incorporated with the physical packages from the Community Atmospheric Model Version 2 (CAM2) of National Center for Atmospheric Research (NCAR), are included.

Keywords: dynamical core, equal-area mesh, anti-symmetry, effective energy conservation.

DOI: 10.1360/04za0001

1 Introduction

The atmospheric model is a necessary tool for climatic studies and weather predictions. Many kinds and many versions of atmospheric models have been developed in the world since the 1980s, such as the NCAR CAM2 that builds on the NCAR Community Climate Model 3 (CCM3)^[1], ECHAM^[2], IAP AGCM^[3–6] and so on. The available models, however, can hardly meet the requirements of further studies on synoptic and climatic problems mainly due to some difficulties in dynamical cores and some uncertainties in model physics, although the model resolution and the description of model physics have been improved greatly following the rapid development of computing technique. To design high-

resolution and high-performance atmospheric models becomes an urgent task in the field of numerical modeling of atmospheric problems, which includes designs of high-performance dynamical cores and further studies on model physical processes. In this paper, only designs of dynamical cores are focused on. Especially, grid-point frameworks are emphasized here. For grid-point frameworks, increase of their resolutions, however, may cause exponentially enhanced high-frequency effects in the Polar Regions and may even lead to computational instabilities in model integrations, due to the singularities of the global atmospheric equations at the Polar Regions. The difference between the grid sizes respectively at the equatorial regions and the Polar Regions will become bigger and bigger, following the increase of horizontal resolutions. It is difficult to find a general-purpose numerical method that can be efficient and computationally stable for getting solutions in both the equatorial regions and the Polar Regions. Therefore, to construct efficient schemes of designing high-resolution dynamical cores for global atmospheric models is more and more important.

Dynamical core is the basic part of a model. A lot of attempts on dynamical cores have been made^[4,7-11]. Generally, there are three kinds of commonly used numerical methods for the design of dynamical cores. These methods are finite difference method, spectral expansion method and semi-Lagrangian method. They have their own merits as well as their own drawbacks. The finite difference method is simple and intuitive, which is easy to be constructed, easy to be coded, easy to be parallelized, easy to keep physical conservations, easy to deal with terrains, easy to nest or be nested, and easy to couple with other components of climate system models. But it is difficult to naturally overcome the singularity and high-frequency effects of the global atmospheric equations at the Polar Regions, and difficult to have a large time step and to run efficiently. The spectral expansion method can overcome the shortcomings of the finite difference method, which can remove the singularity and high-frequency effects of the equations at the Polar Regions, can have a large time step and implement efficiently with the Fast Fourier Transformations (FFT). Especially, this method can reach the best precision for fixed horizontal resolutions. This is why it has been a popular numerical method for design of dynamical cores in recent 20 years. However, it is difficult to deal with some discontinuous variables such as terrains, moisture and so on, and it is hard to be coded and parallelized. The semi-Lagrangian method is for design of a kind of grid-point framework with good stability of the spectral framework. It has the advantages of the finite difference method on dealing with complex terrain, nesting or being nested, coupling with other components of climate system models, as well as the advantage of the spectral expansion method on having large time step. Other problems of this method, however, appear, such as the huge computations for solving an elliptic equation and the difficulties to deal with the particles passing through the poles. Besides the aforesaid three methods, some other numerical methods such as the finite element method and the finite volume method have also been tried for designing dynamical cores. These methods are still under investigation and so far can hardly be applied to numerical modeling of climatic problems and numerical weather predictions.

Corresponding to the numerical methods for solving the global atmospheric equations, there are several mesh systems in common use, which are respectively the equal-interval latitude-longitude mesh for the finite difference method and the semi-Lagrangian method, the Gaussian mesh for the spectral expansion method, the quasi-uniform polygonal mesh for the finite element method and the finite volume method, and other meshes based on the polyhedral approximation, the equal-area mesh and so on. The equal-area mesh is a new mesh for the finite difference method, which will be introduced in the following sections in this paper.

According to the used numerical methods, dynamical cores are mainly classified into three kinds, which are the grid-point framework, the spectral framework and the semi-Lagrangian framework. Models using these frameworks are respectively called the grid-point model, the spectral model and the semi-Lagrangian model. From the above comparisons and discussions on the numerical methods for dynamical cores, it is difficult for us to say which one is the best. Based on the consideration for easily dealing with the complex terrains while keeping some important integral properties of the equations of the global atmosphere, we would like to choose the difference method for designing a new dynamical core for global atmospheric models in this paper. The basic equations after some key variable and independent variable transformations and the analyses on the integral properties of the equations are introduced in Section 2. A weighted equal-area mesh system for overcoming the high-frequency effects of the difference method at the Polar Regions is provided in Section 3. A difference scheme for spatial discretization of the equation set is given and the integral properties of the semi-discretization equations are studied in Section 4. An explicit difference scheme with exact quadratic conservations for the temporal discretization of the semi-discretization equation set is designed in Section 5. Finally, some numerical tests on the new dynamical core regarding its conservations and its integrated performances when coupling with the physical package from NCAR CAM Version 2 are included in Section 6.

2 Basic equations and important integral properties

Consider the hydrostatic balance equations for global baroclinic atmosphere under the colatitude-longitude-pressure coordinates:

$$\begin{aligned}
 \frac{d\mathbf{v}}{dt} &= -\nabla\varphi - f^*\mathbf{k} \times \mathbf{v} + \mathbf{F}, \\
 \frac{dT}{dt} &= \frac{1}{C_p} \frac{RT}{p} \omega + F_T + \frac{1}{C_p} \dot{H}, \\
 \frac{dq}{dt} &= F_q + \dot{Q}_q, \\
 \nabla \cdot \mathbf{v} &= -\frac{\partial \omega}{\partial p}, \\
 \frac{\partial \varphi}{\partial p} &= -\frac{RT}{p},
 \end{aligned} \tag{2.1}$$

where p is the air pressure, \mathbf{v} is the horizontal wind vector, ω is the vertical

velocity, T is the temperature, q is the moisture, φ is the geopotential height, ∇ is the 2-dimensional gradient operator, \mathbf{F} , F_T and F_q are the frictions and dissipations of the motion equations, the thermal equation and the moisture equation respectively, \dot{H} is the source of heat, and \dot{Q}_q is the source of moisture. The horizontal wind vector \mathbf{v} , the gradient operator ∇ , the time global differential quotient and the Coriolis parameter f^* are defined respectively as follows:

$$\begin{aligned} \mathbf{v} &\equiv v\boldsymbol{\theta}^\circ + u\boldsymbol{\lambda}^\circ, \\ \nabla &\equiv \frac{\partial}{a\partial\theta}\boldsymbol{\theta}^\circ + \frac{\partial}{a\sin\theta\partial\lambda}\boldsymbol{\lambda}^\circ, \\ \frac{d}{dt} &\equiv \frac{\partial}{\partial t} + \mathbf{v} \cdot \nabla + \omega \frac{\partial}{\partial p}, \\ f^* &\equiv 2\Omega \cos\theta + \frac{ctg\theta}{a}u, \end{aligned} \quad (2.2)$$

where a is the radius of the earth, Ω is the angular velocity of the earth rotation, θ is the colatitude, λ is the longitude, $\boldsymbol{\theta}^\circ$ and $\boldsymbol{\lambda}^\circ$ are the unit vectors respectively along the direction of colatitude and the direction of longitude. Now, two variable transformations and two coordinate transformations are made on eqs. (2.1). The first variable transformation is the deduction of standard atmospheric stratification. The globally averaged temperature of the standard atmospheric stratification $\tilde{T} = \tilde{T}(p)$ is introduced as the temperature of a standard atmosphere and then the geopotential height $\tilde{\varphi} = \tilde{\varphi}(p)$ is calculated according to the formula of hydrostatic balance: $\frac{d\tilde{\varphi}}{dp} = -\frac{R\tilde{T}}{p}$, where $\tilde{\varphi}(p_0) = 0$, $\tilde{T}(p_0) = 288.15$ K, $p_0 = 1013.25$ hPa. After introducing 1) the deduction of the standard atmosphere^[3,12]:

$$\begin{aligned} T'(\theta, \lambda, p, t) &= T(\theta, \lambda, p, t) - \tilde{T}(p), \\ \varphi'(\theta, \lambda, p, t) &= \varphi(\theta, \lambda, p, t) - \tilde{\varphi}(p), \end{aligned} \quad (2.3)$$

2) the IAP transformations^[3,4,12]:

$$\begin{aligned} (V, U, W, \phi, Q) &\equiv \left(Pv, Pu, P\dot{\sigma}, \frac{PRT'}{\tilde{c}}, p_{es}q \right), \\ P &\equiv \sqrt{p_{es}}, \quad p_{es} = p_s - p_T, \end{aligned} \quad (2.4)$$

3) the vertical coordinate transformation:

$$\sigma = \frac{p - p_T}{p_{es}}, \quad (2.5)$$

and 4) the area coordinate transformation:

$$m = m(\theta), \quad \rho = \rho(\theta) = m'(\theta), \quad (2.6)$$

where p_s is the surface air pressure, p_T is the air pressure at the model top layer, m is a kind of area function with respect to the colatitude θ , and ρ is the area weighting function, then eqs.(2.1) become the following form of basic equations

for global atmosphere under the longitude-area- σ coordinates system:

$$\begin{aligned}
\frac{\partial V}{\partial t} &= - \sum_{n=1}^3 L_n(V) - P_m^{(1)} - P_m^{(2)} + f^*U + PF_m, \\
\frac{\partial U}{\partial t} &= - \sum_{n=1}^3 L_n(U) - P_\lambda^{(1)} - P_\lambda^{(2)} - f^*V + PF_\lambda, \\
\frac{\partial \phi}{\partial t} &= - \sum_{n=1}^3 L_n(\phi) + \frac{\chi}{\sigma P} \left[\tilde{c} + \left(k - \frac{1}{\tilde{c}} \frac{d\tilde{c}}{d \ln p} \right) \frac{\phi}{P} \right] \\
&\quad \cdot (\Omega^{(1)} + \Omega^{(2)} + \Omega^{(3)}) + \frac{RP}{\tilde{c}} F_T + \frac{kP}{\tilde{c}} \dot{H}, \\
\frac{\partial p_{es}}{\partial t} &= -D(P) - \frac{\partial PW}{\partial \sigma}, \\
\frac{\partial \phi'}{\partial \sigma} &= -\frac{\tilde{c}P}{p} \phi, \\
\frac{\partial Q}{\partial t} + \frac{1}{a \sin \theta} \left[\frac{\partial Qu}{\partial \lambda} + \rho \frac{\partial Qv \sin \theta}{\partial m} \right] + \frac{\partial Q}{\partial \sigma} \dot{\sigma} &= p_{es}(F_q + \dot{Q}_q),
\end{aligned} \tag{2.7}$$

where $k \equiv \frac{R}{C_p}$, $\chi \equiv \sigma \frac{P^2}{p} = \frac{p-p_T}{p}$, \tilde{c} is the characteristic velocity of gravity-wave propagation of the standard atmosphere determined by $\tilde{c}^2 \equiv R \left(k\tilde{T} - \frac{d\tilde{T}}{d \ln p} \right)$, L_1 and L_2 are the horizontal advection operators and L_3 is the vertical convection operator, which are defined by

$$\begin{aligned}
L_1(F) &\equiv \frac{1}{2a \sin \theta} \left(2 \frac{\partial Fu}{\partial \lambda} - F \frac{\partial u}{\partial \lambda} \right), \\
L_2(F) &\equiv \frac{\rho}{2a \sin \theta} \left(2 \frac{\partial Fv \sin \theta}{\partial m} - F \frac{\partial v \sin \theta}{\partial m} \right), \\
L_3(F) &\equiv \frac{1}{2} \left(2 \frac{\partial F \dot{\sigma}}{\partial \sigma} - F \frac{\partial \dot{\sigma}}{\partial \sigma} \right),
\end{aligned} \tag{2.8}$$

the gradient force terms are calculated according to the following formulas:

$$\begin{aligned}
P_m^{(1)} &\equiv P \rho \frac{\partial \phi'}{a \partial m}, \\
P_\lambda^{(1)} &\equiv P \frac{\partial \phi'}{a \sin \theta \partial \lambda}, \\
P_m^{(2)} &\equiv 2 \frac{\tilde{c} \chi \phi \rho}{P} \frac{\partial P}{a \partial m}, \\
P_\lambda^{(2)} &\equiv 2 \frac{\tilde{c} \chi \phi}{P} \frac{\partial P}{a \sin \theta \partial \lambda},
\end{aligned} \tag{2.9}$$

and other terms are determined by

$$\begin{aligned}
\Omega^{(1)} &\equiv PW + \sigma \cdot 2P \frac{\partial P}{\partial t}, \\
\Omega^{(2)} &\equiv 2\sigma V \rho \frac{\partial P}{a \partial m}, \\
\Omega^{(3)} &\equiv 2\sigma U \frac{\partial P}{a \sin \theta \partial \lambda}, \\
D(F) &\equiv \frac{1}{a \sin \theta} \left(\rho \frac{\partial FV \sin \theta}{\partial m} + \frac{\partial FU}{\partial \lambda} \right).
\end{aligned} \tag{2.10}$$

The vertical boundary conditions are described as

$$\begin{aligned}
W|_{\sigma=0,1} &= 0, \\
\varphi'|_{\sigma=1} &= \frac{R\tilde{T}_s}{\bar{p}_s} p'_s,
\end{aligned} \tag{2.11}$$

where $\tilde{T}_s \equiv \tilde{T}(p_s)$ and $p'_s \equiv p_s - \tilde{p}_s$. The horizontal boundary conditions are periodic in λ -direction and $u|_{m=m(0)} = u|_{m=m(\pi)} = 0$ in m -direction.

If the forcing and friction terms in eqs. (2.7) are ignored, i.e. $F_\lambda = 0, F_m = 0, F_T = 0, F_q = 0, \dot{H} = 0, \dot{Q}_q = 0$, it is easy to prove that the equations have the following integral properties:

- (1) the total mass conservation: $\frac{\partial}{\partial t} \int_0^{2\pi} \int_{m(0)}^{m(\pi)} p_{es} a^2 \frac{\sin \theta}{\rho} dm d\lambda = 0$;
- (2) the anti-symmetries of the horizontal advection operators L_1 and L_2 and the vertical convection operator L_3 : $\int_0^1 \int_0^{2\pi} \int_{m(0)}^{m(\pi)} FL_n(F) a^2 \frac{\sin \theta}{\rho} dm d\lambda d\sigma = 0$, where $F = U, V, \phi$ and $n=1, 2, 3$;
- (3) the total effective energy conservation:
 $\frac{\partial}{\partial t} \int_0^{2\pi} \int_{m(0)}^{m(\pi)} \left[\int_0^1 \frac{1}{2} (U^2 + V^2 + \phi^2) d\sigma + \frac{R\tilde{T}_s}{\bar{p}_s} \frac{1}{2} (p'_s)^2 \right] a^2 \frac{\sin \theta}{\rho} dm d\lambda = 0$ under the standard stratification approximation: $k - \frac{1}{c} \frac{d\tilde{c}}{d \ln p} = 0$, where $p'_s = p_s - \tilde{p}_s$.

3 Weighted equal-area mesh

In general, the equal-interval colatitude-longitude (or latitude-longitude) mesh is used for the spatial discretization of the equations for global atmosphere for design of global grid-point framework by the finite difference method. The difference scheme with such a mesh, however, has a difficulty at the Polar Regions, which is the singularity at the poles and the high-frequency effects at the neighborhoods of the poles caused by the smaller and smaller zonal grid-sizes when the colatitudes are close to 0° or 180° (or the latitudes close to $\pm 90^\circ$). Especially, exponentially growing high-frequency effects in the Polar Regions will be produced and computational stabilities of the framework may not be ensured, when the horizontal resolutions are increased. For example, a formula to express the change of the minimum zonal grid-size, nearest to the Arctic Pole, with respect to the horizontal resolutions, can be given as the

following:

$$\frac{\Delta l_2}{\Delta l_1} = \frac{a\Delta\lambda_2 \sin(\Delta\theta_2)}{a\Delta\lambda_1 \sin(\Delta\theta_1)} = \left(\frac{\Delta\lambda_2}{\Delta\lambda_1}\right) \cdot \left(\frac{\sin \Delta\theta_2}{\sin \Delta\theta_1}\right). \quad (3.1)$$

If the resolutions double: $\Delta\lambda_2 = \frac{1}{2}\Delta\lambda_1$ and $\Delta\theta_2 = \frac{1}{2}\Delta\theta_1$, the minimum zonal grid-size will be reduced to about one-fourth of the old one: $\frac{\Delta l_2}{\Delta l_1} \approx \frac{1}{4}$ (suppose $\Delta\theta_1$ and $\Delta\theta_2$ are small enough). According to the stability criterion for solutions to hyperbolic-type equations, the time step size will have to be reduced to about one-fourth of the original step size in this case. Therefore, a 2-fold increase of the resolutions will lead to about 16-fold growth of computations, which brings about a big challenge to the present computer conditions.

Another difficulty is the big difference of the grid-sizes between the equatorial regions and the Polar Regions, which causes the difference of computational stability between these two kinds of regions. The stability criterion for solution to hyperbolic-type equations can be written in the following general-utility form:

$$\beta(\theta) = \frac{U_0 \Delta t}{\Delta l_\theta} < \alpha, \quad (3.2)$$

where U_0 is the maximum characteristic velocity, Δt is the time step size, $\Delta l_\theta = a\Delta\lambda \sin \theta$ is the zonal grid-size, θ is the colatitude. Based on expression (3.2), the ratio of stability between the Polar Regions and the equatorial regions can be defined as

$$r = \frac{\beta(\Delta\theta)}{\beta(\pi/2)} = \frac{\Delta l_{\pi/2}}{\Delta l_{\Delta\theta}} = \frac{1}{\sin \Delta\theta}. \quad (3.3)$$

From the above definition, it is easy to know that the higher the horizontal resolutions, the greater the ratio becomes, and thereby the bigger the difference of computational stability between the two kinds of the regions is. For example, when the horizontal resolutions are set to be $0.5^\circ \times 0.5^\circ$, the grid size at the equator is about 55 km, but the size at the zones nearest to the poles is less than 0.5 km. In this case, the ratio of stability is more than 100. If the horizontal resolutions are improved to be $0.1^\circ \times 0.1^\circ$, the two grid sizes will be respectively 11 km and 0.02 km, and the ratio will become more than 500. Table 1 shows the detail information about the change of ratio of stability with respect to the horizontal resolutions. Obviously, the ratio of stability becomes bigger and bigger, following the increase of the horizontal resolutions, which leads to a couple of contradictions between error accumulations in the equatorial regions and computational stabilities in the Polar Regions. The contradictions mean that error accumulations may occur at the equatorial regions due to the too small time step size required to maintain the computational stabilities at the Polar Regions, or computational instabilities may develop at the Polar Regions due to the too large time step size reducing the error accumulations at the equatorial regions. It is difficult to find a general-use numerical method that can be efficient and computationally stable for getting solutions in both the equatorial regions and the Polar Regions. This difficulty is just caused by the unreasonable structure of the equal-interval colatitude-longitude mesh system. Therefore, to construct a good mesh to overcome or mitigate the difficulty is very necessary.

Table 1 Ratio of stability and horizontal resolutions

$\Delta\theta \times \Delta\lambda$	$\Delta l_{\text{equator}}/\text{km}$	$\Delta l_{\text{poles}}/\text{km}$	r
$4^\circ \times 5^\circ$	556.0	39.00	14
$2^\circ \times 2.5^\circ$	278.0	10.00	29
$1^\circ \times 1^\circ$	111.0	2.00	57
$0.5^\circ \times 0.5^\circ$	55.6	0.50	115
$0.25^\circ \times 0.25^\circ$	27.8	0.12	229
$0.1^\circ \times 0.1^\circ$	11.1	0.02	573

Why does the equal-interval colatitude-longitude mesh have the above problem? This is a question we want to answer in this section. Consider a lattice consisting of four grid-points: (θ, λ) , $(\theta, \lambda + \Delta\lambda)$, $(\theta + \Delta\theta, \lambda)$ and $(\theta + \Delta\theta, \lambda + \Delta\lambda)$. The lattice area Δm can be calculated by

$$\Delta m = \Delta l_\theta \cdot (a\Delta\theta) = a^2 \Delta\lambda \Delta\theta \sin \theta. \quad (3.4)$$

It is easily found that the lattice area becomes smaller and smaller at the Polar Regions ($\theta \rightarrow 0^\circ$ or 180°). This may be the key factor causing the high-frequency effects at the Polar Regions. If we construct a new mesh keeping the lattice area constant, the aforesaid difficulties can be overcome. In order to make meridional discretization by the finite difference method conveniently, the new mesh should have the same number of grid-points on each zonal parallel, i.e. $\Delta\lambda$ should be a constant. In this case, $\Delta\theta$ will be changing so that Δm remains unchanged. Ignoring the constants a and $\Delta\lambda$ in expression (3.4), the lattice area can be formulated as a weighted area differential unit Δm :

$$\Delta m = \Delta\theta \sin \theta, \quad (3.5)$$

where the area weighting function is defined by

$$\rho = \rho(\theta) = m'(\theta) = \lim_{\Delta\theta \rightarrow 0} \frac{\Delta m}{\Delta\theta} = \sin \theta, \quad (3.6)$$

From the above formula, the area function can be obtained as

$$m(\theta) = \int_0^\theta \rho(\theta) d\theta = 1 - \cos \theta, \quad \theta \in [0, \pi], \quad m \in [0, 2]. \quad (3.7)$$

With the area weighting function $\rho = \sin \theta$, however, an equal-interval division of the area may produce an unequal-interval division of the colatitude with too large grid-size at the Polar Regions and too small grid-size at the equatorial regions along the θ -direction. For example, if we use the same grid-point number of the equal-interval colatitude-longitude mesh with the horizontal resolutions of $2^\circ \times 2^\circ$, $\Delta\theta$ of the equal-area mesh at the colatitudes next to the poles is 12.1° , while it is only 1.27° as the colatitudes are close to the equator. Too large grid-size at the Polar Regions may seriously affect the modeling of the polar vortex. To mitigate this problem, other proper area weighting function can be used. Here, a new area weighting function is defined as

$$\rho = \rho(\theta) = \begin{cases} 1 - \alpha \left(\left| \frac{\pi}{2} - \theta \right| - \frac{\pi}{3} \right), & \frac{\pi}{3} \leq \left| \frac{\pi}{2} - \theta \right| \leq \frac{\pi}{2}, \\ 1, & \left| \frac{\pi}{2} - \theta \right| < \frac{\pi}{3}, \end{cases} \quad (3.8)$$

where $\alpha = \frac{4}{\pi}$. With this area weighting function, the area function takes the following form:

$$m(\theta) = \int_0^\theta \rho(\theta) d\theta = \begin{cases} \frac{1}{2\alpha} \left\{ \frac{17}{9} - \left[1 - \alpha \left(\theta - \frac{5\pi}{6} \right) \right]^2 \right\} + \frac{2\pi}{3}, & \frac{5\pi}{6} \leq \theta \leq \pi, \\ \frac{1}{2\alpha} \cdot \frac{8}{9} + \left(\theta - \frac{\pi}{6} \right), & \frac{\pi}{6} < \theta < \frac{5\pi}{6}, \\ \frac{1}{2\alpha} \left\{ -\frac{1}{9} + \left[1 - \alpha \left(\frac{\pi}{6} - \theta \right) \right]^2 \right\}, & 0 \leq \theta \leq \frac{\pi}{6}. \end{cases} \quad (3.9)$$

It can be testified that, by using the above area function, an equal-area division can produce an equal-colatitude division at the region: $\frac{\pi}{6} < \theta < \frac{5\pi}{6}$ and an unequal-colatitude division at the high-latitude regions: $0 \leq \theta \leq \frac{\pi}{6}$ and $\frac{5\pi}{6} \leq \theta \leq \pi$. We still use the same grid-point number of the equal-interval colatitude-longitude mesh with the horizontal resolutions of $2^\circ \times 2^\circ$, $\Delta\theta$ of the equal-area mesh at the colatitudes next to the poles is 4.62° , while it is 1.78° at the colatitudes nearest to the equator. Obviously, the meridional grid-size is not too large at the Polar Regions. Therefore, this is a more reasonable weighted equal-area division.

4 Spatial discretization

On the weighted equal-area mesh (3.8)—(3.9), the central difference is used to discretize the terms on the right sides of eqs. (2.7) and the semi-discrete equations is obtained:

$$\begin{aligned} \left[\frac{\partial V}{\partial t} \right]_{i,j+\frac{1}{2},k} &= \left[-\sum_{n=1}^3 L_n(V) - P_m^{(1)} - P_m^{(2)} + f^*U \right]_{i,j+\frac{1}{2},k}, \\ \left[\frac{\partial U}{\partial t} \right]_{i-\frac{1}{2},j,k} &= \left[-\sum_{n=1}^3 L_n(U) - P_\lambda^{(1)} - P_\lambda^{(2)} - f^*V \right]_{i-\frac{1}{2},j,k}, \\ \left[\frac{\partial \phi}{\partial t} \right]_{i,j,k} &= \left[-\sum_{n=1}^3 L_n(\phi) + \frac{\chi}{\sigma P} \left[\tilde{c} + \left(k - \frac{1}{\tilde{c}} \frac{d\tilde{c}}{d \ln p} \right) \frac{\phi}{P} \right] \right. \\ &\quad \left. \cdot (\Omega^{(1)} + \Omega^{(2)} + \Omega^{(3)}) \right]_{i,j,k}, \\ \left[\frac{\partial p_{es}}{\partial t} \right]_{i,j} &= - \left[D(P) + \frac{1}{\Delta\sigma} \delta_\sigma(PW) \right]_{i,j,k}, \\ \frac{1}{\Delta\sigma_k} [\delta_\sigma \phi']_{i,j,k} &= -P_{i,j} \cdot \left[\frac{\tilde{c}\phi}{p} \right]_{i,j,k}, \end{aligned} \quad (4.1)$$

where the terms on the right sides of eqs. (4.1) are determined respectively by

$$\begin{aligned}
[L_1(V)]_{i,j+\frac{1}{2},k} &= \begin{cases} \frac{1}{2a \sin \theta_{j+\frac{1}{2}} \Delta \lambda} [2\delta_\lambda(\bar{V}^\lambda \bar{U}^m) - V\delta_\lambda(\bar{U}^m)]_{i,j+\frac{1}{2},k} \\ (j = 1, 2, \dots, J-1), \\ 0 \quad (j = J), \end{cases} \\
[L_2(V)]_{i,j+\frac{1}{2},k} &= \begin{cases} \frac{\rho_{j+\frac{1}{2}}}{4a \sin \theta_{j+\frac{1}{2}} \Delta m} \cdot V_{i,2\frac{1}{2},k} [(v \sin \theta)_{i,1\frac{1}{2},k} + (v \sin \theta)_{i,2\frac{1}{2},k}] \\ (j = 1), \\ \frac{\rho_{j+\frac{1}{2}}}{2a \sin \theta_{j+\frac{1}{2}} \Delta m} [2(\overline{\overline{v \sin \theta}}^m \overline{\overline{V}}^m)_m - V(\overline{\overline{v \sin \theta}}^m)_m]_{i,j+\frac{1}{2},k} \\ (j = 2, 3, \dots, J-1), \\ 0 \quad (j = J), \end{cases} \\
[L_3(V)]_{i,j+\frac{1}{2},k} &= \begin{cases} \frac{1}{2\Delta\sigma_1} V_{i,j+\frac{1}{2},2} (\bar{\sigma}^m)_{i,j+\frac{1}{2},1\frac{1}{2}} \quad (k = 1), \\ \frac{1}{2\Delta\sigma_k} [2\delta_\sigma(\bar{\sigma}^m \bar{V}^\sigma) - V\delta_\sigma(\bar{\sigma}^m)]_{i,j+\frac{1}{2},k} \\ (k = 2, 3, \dots, K-1), \\ -\frac{1}{2\Delta\sigma_K} V_{i,j+\frac{1}{2},K-1} (\bar{\sigma}^m)_{i,j+\frac{1}{2},K-\frac{1}{2}} \quad (k = K), \end{cases} \quad (4.2) \\
[P_m^{(1)}]_{i,j+\frac{1}{2},k} &= \begin{cases} \frac{\rho_{j+\frac{1}{2}}}{a\Delta m} [\bar{P}^m \cdot (\overline{\overline{\phi}}^\sigma)_m]_{i,j+\frac{1}{2},k} \quad (j = 1, 2, \dots, J-1), \\ 0 \quad (j = J), \end{cases} \\
[P_m^{(2)}]_{i,j+\frac{1}{2},k} &= \begin{cases} \frac{2\rho_{j+\frac{1}{2}}}{a\Delta m} \left[\left(\frac{\tilde{c}\chi\phi}{P} \right)^m P_m \right]_{i,j+\frac{1}{2},k} \quad (j = 1, 2, \dots, J-1), \\ 0 \quad (j = J), \end{cases} \\
[f^*U]_{i,j+\frac{1}{2},k} &= \begin{cases} \left[\overline{\overline{f^*U}}^\lambda \right]_{i,j+\frac{1}{2},k} \quad (j = 1, 2, \dots, J-1), \\ 0 \quad (j = J), \end{cases}
\end{aligned}$$

for the V -dependent equation,

$$\begin{aligned}
[L_1(U)]_{i-\frac{1}{2},j,k} &= \frac{1}{2a \sin \theta_j \Delta \lambda} \left[2 \cdot (\bar{u}^\lambda \bar{U}^\lambda)_\lambda - U \cdot (\bar{u}^\lambda)_\lambda \right]_{i-\frac{1}{2},j,k}, \\
[L_2(U)]_{i-\frac{1}{2},j,k} &= \begin{cases} \frac{\rho_j}{2a \sin \theta_j \Delta m} \left[2\delta_m(\bar{v}^\lambda \sin \theta \bar{U}^m) - U \cdot \delta_m(\bar{v}^\lambda \sin \theta) \right]_{i-\frac{1}{2},j,k} \\ (j = 2, 3, \dots, J-1), \\ 0 \quad (j = 1, J), \end{cases} \\
[L_3(U)]_{i-\frac{1}{2},j,k} &= \begin{cases} \frac{1}{2\Delta\sigma_1} U_{i-\frac{1}{2},j,2} (\bar{\sigma}^\lambda)_{i-\frac{1}{2},j,1\frac{1}{2}} \quad (k=1), \\ \frac{1}{2\Delta\sigma_k} \left[2\delta_\sigma(\bar{\sigma}^\lambda \bar{U}^\sigma) - U \cdot \delta_\sigma(\bar{\sigma}^\lambda) \right]_{i-\frac{1}{2},j,k} \\ (k=2, 3, \dots, K-1), \\ -\frac{1}{2\Delta\sigma_K} U_{i-\frac{1}{2},j,K-1} (\bar{\sigma}^\lambda)_{i-\frac{1}{2},j,K-\frac{1}{2}} \quad (k=K), \end{cases} \quad (4.3) \\
[P_\lambda^{(1)}]_{i-\frac{1}{2},j,k} &= \frac{1}{a \sin \theta_j \Delta \lambda} \left[\bar{P}^\lambda \cdot (\bar{\varphi}^\sigma)_\lambda \right]_{i-\frac{1}{2},j,k}, \\
[P_\lambda^{(2)}]_{i-\frac{1}{2},j,k} &= \frac{2}{a \sin \theta_j \Delta \lambda} \left[\left(\frac{\tilde{c}\chi\phi}{P} \right)^\lambda P_\lambda \right]_{i-\frac{1}{2},j,k}, \\
[f^*V]_{i-\frac{1}{2},j,k} &= \begin{cases} \left[\frac{f^*}{\sin \theta} (\bar{V}^\lambda \sin \theta)^m \right]_{i-\frac{1}{2},j,k} \quad (j = 2, 3, \dots, J-1), \\ 0 \quad (j = 1, J), \end{cases}
\end{aligned}$$

for the U -dependent equation,

$$\begin{aligned}
[L_1(\phi)]_{i,j,k} &= \frac{1}{2a \sin \theta_j \Delta \lambda} \left[2\delta_\lambda(u\bar{\phi}^\lambda) - \phi\delta_\lambda u \right]_{i,j,k}, \\
[L_2(\phi)]_{i,j,k} &= \begin{cases} \frac{2\rho_{1\frac{1}{2}}}{Ia\Delta m} \sum_{i=1}^I \left[v_{i,1\frac{1}{2},k} \cdot \phi_{i,2,k} \right] \quad (j=1), \\ \frac{\rho_j}{2a \sin \theta_j \Delta m} \left[2\delta_m(v \sin \theta \bar{\phi}^m) - \phi\delta_m(v \sin \theta) \right]_{i,j,k} \\ (j=2, 3, \dots, J-1), \\ -\frac{2\rho_{J-\frac{1}{2}}}{Ia\Delta m} \sum_{i=1}^I \left[v_{i,J-\frac{1}{2},k} \cdot \phi_{i,J-1,k} \right] \quad (j=J), \end{cases}
\end{aligned}$$

$$\begin{aligned}
[L_3(\phi)]_{i,j,k} &= \begin{cases} \frac{1}{2\Delta\sigma_1} \dot{\sigma}_{i,j,1\frac{1}{2}} \phi_{i,j,2} & (k=1), \\ \frac{1}{2\Delta\sigma_k} \left[2\delta_\sigma \left(\dot{\sigma} \overline{\phi}^\sigma \right) - \phi \delta_\sigma(\dot{\sigma}) \right]_{i,j,k} & (k=2, 3, \dots, K-1), \\ -\frac{1}{2\Delta\sigma_K} \dot{\sigma}_{i,j,K-\frac{1}{2}} \phi_{i,j,K-1} & (k=K), \end{cases} \\
[\Omega^{(1)}]_{i,j,k} &= \left[P \overline{\overline{W}}^\sigma + \sigma \frac{\partial p_{es}}{\partial t} \right]_{i,j,k}, \\
[\Omega^{(2)}]_{i,j,k} &= \begin{cases} \frac{2\rho_j \sigma_k}{a \sin \theta_j \Delta m} \left[\overline{V \sin \theta P_m^m} \right]_{i,j,k} & (j=2, 3, \dots, J-1), \\ \frac{4\rho_{1\frac{1}{2}} \sigma_k}{Ia \Delta m} \sum_{i=1}^I [VP_m]_{i,1\frac{1}{2},k} & (j=1), \\ \frac{4\rho_{J-\frac{1}{2}} \sigma_k}{Ia \Delta m} \sum_{i=1}^I [VP_m]_{i,J-\frac{1}{2},k} & (j=J) \end{cases} \\
[\Omega^{(3)}]_{i,j,k} &= \frac{2\sigma_k}{a \sin \theta_j \Delta \lambda} \left[\overline{UP_\lambda}^\lambda \right]_{i,j,k},
\end{aligned} \tag{4.4}$$

for the ϕ -dependent equation and

$$\begin{aligned}
[D(P)]_{i,j,k} &= \begin{cases} \frac{4\rho_{1\frac{1}{2}}}{Ia \Delta m} \sum_{i=1}^I [(V\overline{P^m})_{i,1\frac{1}{2},k}] & (j=1), \\ \frac{1}{a \sin \theta_j} \left[\frac{1}{\Delta \lambda} \delta_\lambda(U\overline{P^\lambda}) + \frac{\rho_j}{\Delta m} \delta_m(V \sin \theta \overline{P^m}) \right]_{i,j,k} & (j=2, 3, \dots, J-1), \\ -\frac{4\rho_{J-\frac{1}{2}}}{Ia \Delta m} \sum_{i=1}^I [(V\overline{P^m})_{i,J-\frac{1}{2},k}] & (j=J), \end{cases} \\
\left[\frac{\partial PW}{\partial \sigma} \right]_{i,j,k} &= \left[\frac{1}{\Delta \sigma} \delta_\sigma(PW) \right]_{i,j,k},
\end{aligned} \tag{4.5}$$

for the continuity equation. In the above formulas, some operations are used, which are respectively defined in the following. 1) Discrete functions on $[a, b]$ are defined by

$$\begin{aligned}
F_l &\equiv F(r_l), \quad r_l = a + (l-1)\Delta r, \\
G_{l+\frac{1}{2}} &\equiv G\left(r_{l+\frac{1}{2}}\right), \quad r_{l+\frac{1}{2}} = a + \left(l - \frac{1}{2}\right) \Delta r,
\end{aligned} \tag{4.6}$$

where $\Delta r = \frac{b-a}{L}$, $l = 1, 2, \dots, L+1$.

2) Two difference operators are defined by

$$\begin{aligned}(F_r)_{l+\frac{1}{2}} &\equiv F_{l+1} - F_l, \\ (\delta_r G)_l &\equiv G_{l+\frac{1}{2}} - G_{l-\frac{1}{2}}.\end{aligned}\quad (4.7)$$

And 3) two average operators are defined by

$$\begin{aligned}(\bar{F}^r)_{l+\frac{1}{2}} &\equiv \frac{1}{2}(F_{l+1} + F_l), \\ (\bar{\bar{G}})_l &\equiv \frac{1}{2}(G_{l+\frac{1}{2}} + G_{l-\frac{1}{2}}).\end{aligned}\quad (4.8)$$

For the horizontal discretization above, the Arakawa C structure is used in the weighted equal-area mesh. With the Arakawa C-structure, zonal wind $u_{i,j}$ is defined on the position of $(\lambda_{i-\frac{1}{2}}, \theta_j)$, meridional wind $v_{i,j}$ is defined on the position of $(\lambda_i, \theta_{j+\frac{1}{2}})$ and other variables such as temperature, surface pressure, moisture and so on are defined on the position of (λ_i, θ_j) . While for the vertical discretization, a similar structure is used, with which, only the vertical velocity $\dot{\sigma}_k$ and the geopotential height deviation φ'_k are at the altitude of σ_k , others are at the altitude of $\sigma_{k+\frac{1}{2}}$. In addition, p_T is at the model top: $\sigma = 0$, and p'_s, \tilde{T}_s are at the model surface: $\sigma = 1$. It can be verified that eqs. (4.1) have 4 integral properties. First, the equations keep the mass conservation constant without any corrections:

$$\frac{\partial}{\partial t} \sum_{i=1}^I \sum_{j=1}^J [p_{es}]_{i,j} \cdot a^2 \in_j \Delta m \Delta \lambda = 0, \quad (4.9)$$

where

$$\in_j = \begin{cases} \frac{\rho_{1\frac{1}{2}}^{-1}}{4} \sin \theta_{1\frac{1}{2}} & (j = 1), \\ \rho_j^{-1} \sin \theta_j & (j = 2, 3, \dots, J-1), \\ \frac{\rho_{J-\frac{1}{2}}^{-1}}{4} \sin \theta_{J-\frac{1}{2}} & (j = J), \end{cases} \quad (4.10)$$

and

$$\in_{j+\frac{1}{2}} = \begin{cases} \rho_{j+\frac{1}{2}}^{-1} \sin \theta_{j+\frac{1}{2}} & (j = 1, 2, \dots, J-1), \\ 0 & (j = J). \end{cases} \quad (4.11)$$

Next, the discrete advection operators L_1, L_2 and the convection operator L_3 are all anti-symmetric:

$$\sum_{k=1}^K \sum_{j=1}^J \sum_{i=1}^I [F \cdot L_1(F)]_{i,j+j_0,k} \cdot a^2 \in_{j+j_0} \Delta \lambda \Delta m \Delta \sigma_k = 0,$$

$$\begin{aligned}
& \sum_{k=1}^K \sum_{j=1}^J \sum_{i=1}^I [F \cdot L_2(F)]_{i,j+j_0,k} \cdot a^2 \in_{j+j_0} \Delta\lambda \Delta m \Delta\sigma_k = 0, \\
& \sum_{k=1}^K \sum_{j=1}^J \sum_{i=1}^I [F \cdot L_3(F)]_{i,j+j_0,k} \cdot a^2 \in_{j+j_0} \Delta\lambda \Delta m \Delta\sigma_k = 0. \tag{4.12}
\end{aligned}$$

$$j_0 = \begin{cases} 0 & \text{when } F = U, \phi, \\ \frac{1}{2} & \text{when } F = V. \end{cases}$$

Thirdly, the Coriolis force in the semi-discrete equations does no work globally:

$$\begin{aligned}
& \sum_{i=1}^I \sum_{j=1}^J [f^* V]_{i-\frac{1}{2},j,k} \cdot U_{i-\frac{1}{2},j,k} \cdot a^2 \in_j \Delta m \Delta\lambda \\
& - \sum_{i=1}^I \sum_{j=1}^J [f^* U]_{i,j+\frac{1}{2},k} \cdot V_{i,j+\frac{1}{2},k} \cdot a^2 \in_{j+\frac{1}{2}} \Delta m \Delta\lambda = 0. \tag{4.13}
\end{aligned}$$

Finally, the equations maintain the effective energy conservation:

$$\begin{aligned}
& \frac{\partial}{\partial t} \left\{ \sum_{k=1}^K \left[\sum_{i=1}^I \sum_{j=1}^J \left(\frac{1}{2} U^2 \right)_{i-\frac{1}{2},j,k} \cdot a^2 \in_j \Delta m \Delta\lambda \right. \right. \\
& + \sum_{i=1}^I \sum_{j=1}^J \left(\frac{1}{2} V^2 \right)_{i,j+\frac{1}{2},k} \cdot a^2 \in_{j+\frac{1}{2}} \Delta m \Delta\lambda \\
& + \sum_{i=1}^I \sum_{j=1}^J \left(\frac{1}{2} \phi^2 \right)_{i,j,k} \cdot a^2 \in_j \Delta m \Delta\lambda \left. \right] \Delta\sigma_k \\
& + \sum_{i=1}^I \sum_{j=1}^J \left[\frac{R\tilde{T}_s}{\tilde{p}_s} \frac{1}{2} (p'_s)^2 \right]_{i,j} \cdot a^2 \in_j \Delta m \Delta\lambda \left. \right\} = 0 \tag{4.14}
\end{aligned}$$

under the standard stratification approximation: $k - \frac{1}{\bar{c}} \frac{d\bar{c}}{d \ln p} = 0$.

5 Temporal discretization

After the spatial discretization is completed, the temporal discretization is taken into account in this section. Here, the explicit difference scheme with exact quadratic conservations developed by Wang et al.^[6] is generalized to solve the semi-discrete equations (4.1). For this aim, the equations are rewritten into the operator form:

$$\left[\frac{\partial \mathbf{F}}{\partial t} \right]_{i,j,k} = [L\mathbf{F}]_{i,j,k}, \tag{5.1}$$

where

$$[\mathbf{F}]_{i,j,k} = \left[V_{i,j+\frac{1}{2},k}, U_{i-\frac{1}{2},j,k}, \phi_{i,j,k}, (p_{es})_{i,j} \right]^T, \tag{5.2}$$

and

$$[L\mathbf{F}]_{i,j,k} = \begin{bmatrix} \left[-\sum_{n=1}^3 L_n(V) - P_m^{(1)} - P_m^{(2)} + f^*U \right]_{i,j+\frac{1}{2},k} \\ \left[-\sum_{n=1}^3 L_n(U) - P_\lambda^{(1)} - P_\lambda^{(2)} - f^*V \right]_{i-\frac{1}{2},j,k} \\ \left[-\sum_{n=1}^3 L_n(\phi) + \frac{\chi}{\sigma P} \left[\tilde{c} + \left(k - \frac{1}{\tilde{c}} \frac{d\tilde{c}}{d \ln p} \right) \frac{\phi}{P} \right] \cdot (\Omega^{(1)} + \Omega^{(2)} + \Omega^{(3)}) \right]_{i,j,k} \\ - [D(P) + \frac{1}{\Delta\sigma} \delta_\sigma(PW)]_{i,j,k} \end{bmatrix}. \quad (5.3)$$

According to (4.12), L is an anti-symmetrical operator:

$$(L\mathbf{F}, \mathbf{F}) = 0, \quad (5.4)$$

when $k - \frac{1}{\tilde{c}} \frac{d\tilde{c}}{d \ln p} = 0$, where the discrete inner product is defined by

$$\begin{aligned} (\mathbf{F}_1, \mathbf{F}_2) = & \frac{1}{2} \sum_{i=1}^I \sum_{j=1}^J \left[\sum_{k=1}^K \left\langle (U_1 \cdot U_2)_{i-\frac{1}{2},j,k} + (V_1 \cdot V_2)_{i,j+\frac{1}{2},k} \cdot \frac{\epsilon_{j+\frac{1}{2}}}{\epsilon_j} + (\phi_1 \cdot \phi_2)_{i,j,k} \right\rangle \Delta\sigma_k \right. \\ & \left. + \left\langle \frac{RT_s}{\tilde{p}_s} (p'_{s1} \cdot p'_{s2}) \right\rangle_{i,j} \right] \epsilon_j. \end{aligned} \quad (5.5)$$

Thus, the effective energy conservation of eqs. (5.1) or (4.1) can be kept in the case $k - \frac{1}{\tilde{c}} \frac{d\tilde{c}}{d \ln p} = 0$, when the explicit difference scheme with exact quadratic conservations^[6]

$$\begin{aligned} \mathbf{F}^{n+1} &= \mathbf{F}^n + \tau_n A \mathbf{F}^n, \\ A \mathbf{F}^n &= \frac{1}{12} [5L\tilde{\mathbf{F}} + 8L\mathbf{F}^n - L\mathbf{F}^{n-1}], \\ \tilde{\mathbf{F}} &= \mathbf{F}^{n-1} + 2\tau L\mathbf{F}^n \end{aligned} \quad (5.6)$$

is applied to solve eqs. (5.1) or (4.1), where τ is the guess of time step size, τ_n is the corrected time step size for each-step integration:

$$\begin{aligned} \tau_n &= \frac{\tau}{6 \|\mathbf{A}\mathbf{F}^n\|^2} [5(L\tilde{\mathbf{F}}, \tilde{R}_1) + (L\mathbf{F}^{n-1}, \tilde{R}_2)], \\ \tilde{R}_1 &= \frac{\tilde{\mathbf{F}} - \mathbf{F}^n}{\tau}, \quad \tilde{R}_2 = \frac{\mathbf{F}^n - \mathbf{F}^{n-1}}{\tau}. \end{aligned} \quad (5.7)$$

Now, a full-discrete scheme for the motion equations, the thermal equation and the continuity equation is established. The moisture equation, however, has not been considered. For solving this kind of advection equation, Yu^[13] developed the two-step shape-preserving advection scheme, which has been successfully applied in operational weather predictions and atmospheric researches. A lot of applications of this scheme by about 30 weather stations and institutes in China and some Asian countries show its good performances. Thus, it is generalized to solve the global moisture equation on the weighted equal-area mesh. By using the full-discrete scheme constructed in this paper and the generalized advection scheme, a new parallel dynamical core is coded. Theoretically, the dynamical core has a flexibly adjustable horizontal and vertical resolutions, and

is computationally stable without any filtering or smoothing in the Polar Regions. Especially, it keeps the mass conservation unchanged and conserves the effective energy under the standard stratification approximation, which will be tested in the following section.

6 Numerical tests

In order to assess the performance of the new dynamical core designed above, two numerical tests are made respectively by using 240 processors and 80 processors on the computer platforms of LSSC II and IAP1800. The first test is to examine the mass conservation and the effective energy conservation of the dynamical core. The vertical resolution is set to be 26 layers, from the earth surface to the altitude where the pressure is 2.19 hPa. The horizontal resolutions are $2^\circ \times 2^\circ$. The guess of time step size is 150 s. The initial conditions are interpolated from NCEP/NCAR re-analyses. The real terrains are considered in the dynamical core. Table 2 shows the evolutions of the total mass, the total effective energy and the corrected time step size from a one-year integration under the standard stratification approximation, starting from January 1, 1998. From the table, it can be easily found that the dynamical core does conserve the total mass and the total effective energy exactly. The corrected time step sizes are always greater than but very close to the guess of time step size, which means a good stability of the new dynamical core.

Table 2 Evolutions of the mass, the effective energy and the time step size

Time	Global mass/hPa	Global effective energy/ $\text{m}^2 \cdot \text{hPa} \cdot \text{s}^{-2}$	Time step size $\tau_n (\tau = 150 \text{ s})$
Jan. 1, 1998	10074379.2210984	18792458336.9517	151.174810998735
Feb. 1, 1998	10074379.2210984	18792458336.9517	151.185492971827
Mar. 1, 1998	10074379.2210984	18792458336.9517	151.236218691828
Apr. 1, 1998	10074379.2210984	18792458336.9516	151.240532206824
May 1, 1998	10074379.2210984	18792458336.9515	151.231141155487
Jun. 1, 1998	10074379.2210984	18792458336.9515	151.243892928978
Jul. 1, 1998	10074379.2210984	18792458336.9514	151.229072155714
Aug. 1, 1998	10074379.2210984	18792458336.9514	151.220593084076
Sep. 1, 1998	10074379.2210984	18792458336.9513	151.216573998333
Oct. 1, 1998	10074379.2210984	18792458336.9512	151.230595270230
Nov. 1, 1998	10074379.2210984	18792458336.9512	151.222462288386
Dec. 1, 1998	10074379.2210984	18792458336.9511	151.221795523045

Another test is to examine the integrated performance of the dynamical core when it couples with the model physics from the NCAR CAM2. Actually, the coupling of the dynamical core and the model physics leads to the birth of a new AGCM. With the same resolutions, the same parameters for model physics and the same initial conditions, the new AGCM and the NCAR CAM2 completed 11-year seasonal runs respectively. Fig. 1 gives the global distributions of climatically averaged precipitations respectively from (a) Xie & Arkin Analysis of Precipitation regarded as a kind of observation data, (b) the later 10-year results by the new AGCM and (c) the later 10-year results by the NCAR CAM2.

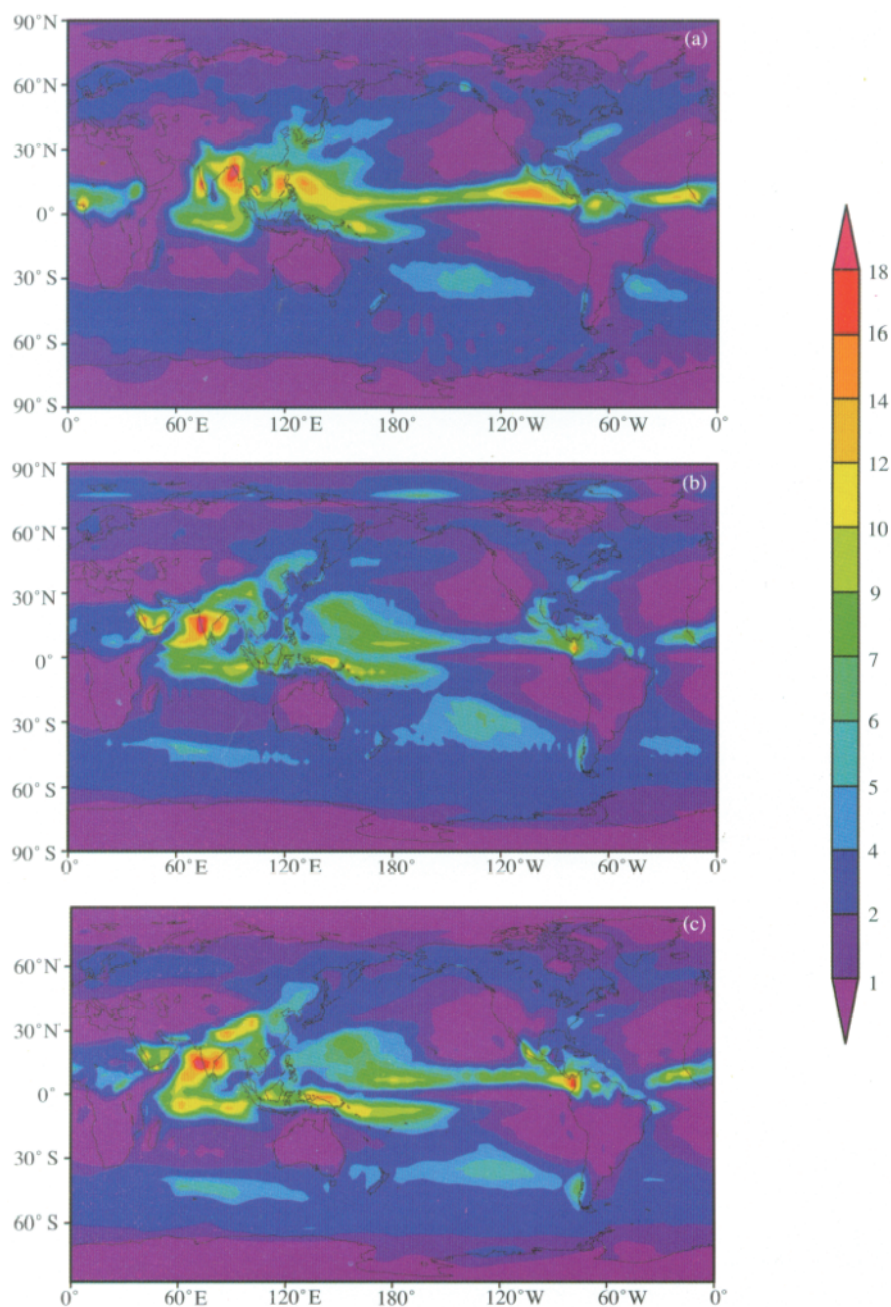


Fig. 1. Global summer precipitation from (a) Xie & Arkin data; (b) the 11-year integration by the new AGCM; (c) the 11-year integration by the NCAR CAM2.

Comparing the results from the new AGCM and the NCAR CAM2 with the observation data, we can find that, the simulations from two models are all like the observations in pattern. But, the NCAR CAM2 produced a long false little-rain zone in the west tropic Pacific Ocean, which extends too westerly. The new

AGCM improved the results obviously in this area. Another key improvement by the new AGCM is the better simulations of precipitation at the northeastern side of the Tibet Plateau. The precipitations by the NCAR CAM2 in this area are too strong. The negative terrain produced by the spectral expansion may be one of the main factors causing the above problems in the NCAR CAM2. The finite difference scheme can describe the terrain well and hereby the new AGCM can reduce the problems. Because two models have the same physics, but different dynamical cores, the improvements by the new model are mainly due to the dynamical core. It means that the new dynamical core has better performances than the spectral dynamical core used in NCAR CAM2 does. Of course, there are still many problems in both models, such as the simulations of precipitation in the monsoon area, which cannot be improved only by dynamical cores. Further studies should be focused on model physics. The comparisons here are only to verify the good performance of the new dynamical core.

Acknowledgements This paper is supported by the 973 Project (Grant No. G1999032801), the Fund for Innovative Research Groups (Grant No. 41221503) and the National Natural Science Foundation of China (Grant No. 40233031).

References

1. Kiehl, J. T., Gent, P. R., Bonan, G. B. et al., Description of the NCAR Community Climate Model (CCM3), NCAR Tech. Note NCAR/TN-420 + STR, 1996, 152 pp.
2. Roeckner, E., Arpe, K., Bengtsson, L. et al., The atmospheric general circulation model ECHAM-4: model description and simulation of present-day climate, Max-Planck-Institut Fur Meteorologie Report No. 218, 1996, 90pp.
3. Wang Bin, Ji Zhongzhen, An economical consistent dissipation operator and its application to the improvement of AGCM, *Advances in Atmospheric Sciences*, 1997, 14(1): 53—58.
4. Wu, G., Liu, H., Zhao Y. et al., A nine-layer atmospheric general circulation model and its performance, *Adv. Atmos. Sci.*, 1996, 13(1): 1—18.
5. Zeng, Q., Zhang, X., Liang, X. et al., Documentation of IAP Two-Level Atmospheric General Circulation Model, DOE/ER/60314-H1, TR044, 1989, 383pp.
6. Zhang, X. -H., Dynamical framework of IAP nine-level atmospheric model, *Advances in Atmospheric Sciences*, 1990, 7(1): 67—77.
7. Chen, Minghang, Rood, R. B., Takacs, L. L., Impact of a semi-Lagrangian and an Eulerian dynamical core on climate simulations, *Journal of Climate*, Boston, 1997, 10(9): 2374—2389.
8. Fox-Rabinovitz, M. S., Stenchikov, G. L., Suarez, M. J. et al., A uniform- and variable-resolution stretched-grid GCM dynamical core with realistic orography, *Monthly Weather Review*, 2000, 128(6): 1883—1898.
9. Held, I. M., Suarez, M. J., A proposal for the intercomparison of the dynamical cores of atmospheric general circulation models, *Bulletin of the American Meteorological Society*, Boston, 1994, 75(10): 1825—1830.
10. Ringler, T. D., Heikes, R. P., Randall, D. A., Modeling the atmospheric general circulation using a spherical geodesic grid: a new class of dynamical cores, *Monthly Weather Review*, 2000, 128(7): 2471—2490.
11. Rivier, L., Loft, R., Polvani, L. M., An efficient spectral dynamical core for distributed memory computers, *Mon. Weather Rev.*, 2002, 130(5): 1384—1396.
12. Zeng, Q., Zhang, X., Finite difference scheme keeping the effective energy conservation of the spherical primitive equation set for the baroclinic atmosphere, *Chinese Journal of Atmospheric Sciences*, 1987, 11(2): 113—127.
13. Yu, R., A two-step shape-preserving advection scheme, *Advances in Atmospheric Sciences*, 1994, 11(4): 479—490.